An Adaptive and Multifunctional DC-DC Converter for Onshore Ship Charging

Sohaib Qazi[a,b], Prasanth Venugopal[a], Gert Rietveld[a,c], Alan J. Watson[b], Patrick Wheeler[b], Thiago Batista Soeiro[a]
[a]Power Electronics and Electromagnetic Compatibility Group, University of Twente, Enschede, The Netherlands
[b]Power Electronics, Machines and Control Group, University of Nottingham, Nottingham, United Kingdom
[c]Department of Electricity and Time, Van Swinden Laboratorium, Delft, The Netherlands
Email: *sohaib.qazi@utwente.nl*

***Abstract*—Maritime electrification is a critical upgrade to enable sustainable and environmentally friendly shipping. Therefore, in recent years, there has been a significant interest in the development of battery-based boats and ferries. A key element for the reliable operation of these vessels is the onshore charging interface. Unlike in electric cars, the onboard power system and the operating voltage in different vessels can vary over a significantly large range. Therefore, the development of a multi-functional charging unit can be challenging. This paper proposes a new power electronics converter that comprises an adaptable charging interface that can operate efficiently over a very wide range of output voltage, and deliver power to different vessels. Simulation results are presented to illustrate the operation of the proposed circuit.**

***Index Terms*—DC-DC converter, e-mobility, fast-charging, resonant converter, shore-to-ship power**

I. Introduction

In recent years, the use of dc-based distribution systems onboard has gained popularity in the development of maritime transportation. Elimination of extra stages of ac/dc conversion in propulsion drives, an easier amalgamation of dc-based energy sources like batteries packs, fuel cells, and PV arrays as well as the development of fast and reliable solid-state breakers have favored the switch to predominantly dc architecture onboard, especially in smaller vessels like boats and ferries [1]. Therefore, onshore charging of these vessels typically involves the use of high-power converters at the shore with a dc output that is connected to the main bus onboard (Fig. 1). The onshore power electronics framework needed for the fast charging of battery-based vessels may still differ depending on the port power system attributes such as voltage levels, possible use of onshore batteries, presence of a dc shore bus, and so on [2], [3]. In conventional systems, galvanic isolation from the MV grid is provided by a line-frequency transformer (LFT) which is subsequently connected to stages of ac/dc and dc/dc conversion for delivering power to the ship bus. With the development of efficient semiconductor technologies, solid-state transformers (SSTs) have emerged as feasible alternatives to the LFTs for providing isolation as they offer a significant increase in power density while maintaining decent efficiency. Therefore, the use of low-weight and low-volume SSTs has been extensively explored in powering traction systems and for charging electric vehicles [4]. With imminent large-scale electrification of boats and ferries on the horizon, employing SSTs in the shore environment can enable the use of modular and compact shore charging stations for these vessels. In order to increase the return on investment and reduce capital expenditure of electrification, ship manufacturers deploy onshore chargers capable of delivering energy to different vessels. However, the operating voltage of the onboard dc system can vary significantly depending on the size and type of the vessel. Typically, the onboard bus voltages in battery-based ferries are less than 1500 V with most vessels employing 400-1000 V systems on board. Therefore, a multi-functional charging station capable of efficiently delivering power across such a wide-voltage range can be quite difficult to design.

Unlike the design for car charging technology, there is not a lot of literature focusing specifically on shore power converters feeding electric ships. In typical fast charging systems, phase-shift full-bridge converters are commonly used which operate with a buck-type regulation. Therefore, they deliver energy most efficiently when the output voltage is maximum and the phase shift between the full-bridge legs is the least [5]. Over the years, other variants of the full-bridge topology have been developed to improve efficiency over a wider range by extending the operation of zero-voltage switching (ZVS) and/or zero-current switching (ZCS). In particular, resonant converters have been extensively analyzed [6], [7] wherein the switching frequency can be varied to attain a converter gain across a wide voltage range. However, this can lead to poor regulation and unstable operation at lighter loads. Dual control in resonant converters, as presented in [8], combine phase-shift and variable frequency controls enabling a narrower operating frequency band and tight controllability of the power injection into the battery for the whole charging cycle. In [9]–[11], isolated dc/dc converters featuring reconfigurability of the transformer secondary-side windings are presented for both the phase-shift and resonant converters. Therein, the system can be designed to operate with a similar phase shift control angle in two voltage ranges: the lower voltage range (with the transformer secondaries paralleled) or the higher voltage range (transformer secondaries in series). This is essential to reduce the circulating power necessary to control the power injection of the converter, which will improve the power conversion efficiency of the system. This paper proposes the isolated dc/dc converters shown in Fig. 2 (a), (b) (LLC resonant-based converter) and Fig. 2

This work is supported by the Marie Skłodowska-Curie Actions European Joint Doctoral Network - ETUT and has received funding from the European Union's Horizon 2020 Research and Innovation program under grant agreement no. 955646.

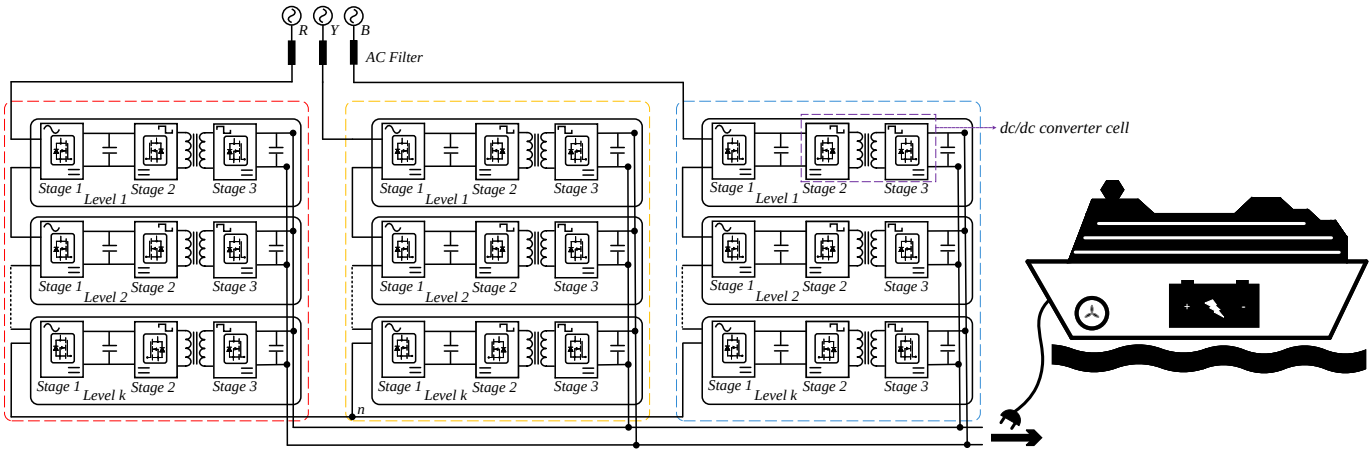

Fig. 1. A cascaded H-bridge fed SST for onshore-charging of battery-based ships; the dc/dc converter cells enable medium frequency isolation.

(c), (d) (phase-shift-based converter). This circuit comprises of two dc/dc converters intricately arranged to create three voltage range operations where the pulse frequency modulation (PFM) of the full bridges can be used for voltage regulation. The circuit is therefore able to retain the ZVS turn-on for the primary-side switches in the three output voltage ranges and minimize the maximum voltage stress at the secondary side diodes. These features enable an excellent power efficiency operation for a wide output voltage range.

II. Operation of the Proposed DC/DC Converter

The proposed converter, as shown in Fig. 2, features circuit reconfigurability provided by the auxiliary switches S_1, S_2 and S_3 at the secondary side, i.e., when S_1 is ON, both S_2 - S_3 will be OFF setting the left and right rectifying bridges in series. On the other hand, when S_1 is OFF, both S_2 and S_3 (switches or diodes) will be ON, setting the left and right rectifying bridges in parallel. Additionally, the three bridge rectifying sides can be used to interconnect the two secondary sides of the transformers in series or in parallel, leading to a voltage or current doubling equivalent circuit at the output, respectively. This can be achieved by the phase-shift alignment (in-phase or anti-phase) of the transformer's primary side full-bridge converters.

The interconnections on the secondary side help in achieving voltage quadrupling when the reconfiguration switch S_1 is on while S_2 and S_3 are off. Under this condition, when the primary side bridges operate exactly in phase, the secondary diodes D_{1a} and D_{6a}, and D_{1b} and D_{6b} all appear in series (for the positive half cycle of transformer secondary voltage) such that the load voltage V_{out} is $4V_i$ where V_i is the magnitude of voltage reflected across the secondary and tertiary windings ($V_i = V_{p1}/n = V_{p2}/n$). This condition (Mode I) corresponds to the maximum voltage achievable at the output terminals as depicted in Fig. 3 (a). Conversely, in Mode II, S_1 is kept OFF while S_2 and S_3 are kept ON. The load voltage V_{out} equals to $2V_i$ with the primary-side full-bridges operating in phase (D_{1a} and D_{6a} appear in series and their combination is paralleled with D_{1b} and D_{6b}) as shown in Fig. 3 (b).

In Mode III, the primary side bridges operate completely anti-phase and the output voltage equals $2V_i$ when S_1 is ON and S_2, S_3 are kept OFF (Fig. 3 (c)). By keeping the anti-phase operation of the full-bridge converters and reversing the switching state of the auxiliary switches (S_1 is OFF and S_2, S_3 are kept ON), the output voltage equals V_i (Mode IV) and the converter delivers maximum current to the load as shown in Fig. 3 (d). Note that the anti-phase operation of the full-bridge converters governs the conduction of the central leg diodes (D_{3a}, D_{4a}, D_{3b}, D_{4b}) which will carry twice the current of the non-central leg diodes. Therefore, these diodes may be assembled by paralleling two diodes of the same rating as used in the non-central legs. Under this condition, the current should be ideally shared by the two primary modules equally.

Additional voltage regulation can be achieved by two degrees of freedom in relation to the implementation of a phase-shift control: by adjusting the phase-shift between the compounding bridge legs of the full-bridge converters (while keeping the phase-shift between the two full-bridge converters statically in phase or anti-phase); or by adjusting the phase-shift between the two full-bridge converters (while operating each full-bridge converter with a bipolar modulation which leads to the highest equivalent duty cycle); or by a combination of these two phase-shift control strategies. The first option utilizes the operation of the zero voltage (or free-wheeling state) of the full-bridge converter equivalently to a unipolar modulation which can be used to control the equivalent duty cycle seen on the output side. The second option can be used to reduce the duration for which the diodes at the secondary side rectification appear in series or parallel and thereby it will affect the average voltage over a switching cycle. This operation will affect the power-sharing between the two full-bridge converters, wherein evenly shared power is only achieved if the two inverters operate in phase or anti-phase assuming that the equivalent duty cycle of each circuit is the same. Furthermore, an intermediate phase shift can lead to an operation with additional secondary-side equivalent circuits where the conducting paths may differ from

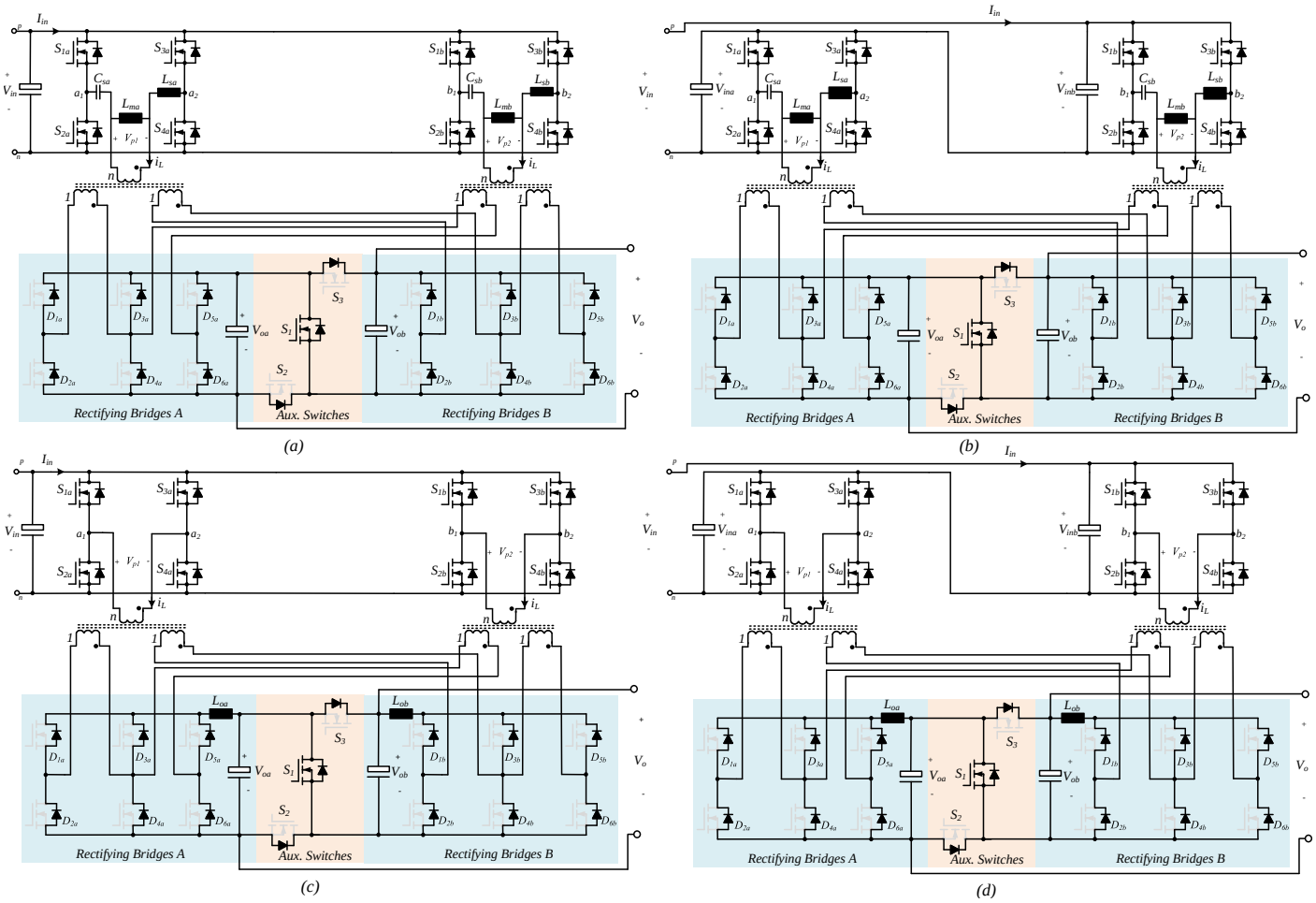

Fig. 2. Circuit topology of the proposed converter configured as an LLC resonant converter where the compounding full-bridges converters are connected in (a) parallel; (b) series. The proposed converter is configured as a phase-shift converter where the compounding converters are connected in (c) parallel; and (d) series. Note that the secondary diodes could be assembled with MOSFETS operated in synchronous rectification for reducing semiconductor conduction losses. Also, note that the auxiliary semiconductors can be assembled with mechanical switches.

the ones shown in Fig. 3.

When the circuit is configured as an LLC resonant converter, naturally, the variation of switching frequencies of the full bridges can still be used to alter the gain of the converter. In that case, the reconfigurability enables narrowing the switching frequency range for yielding a wide range of output voltage. If the phase-shift of the converter is restricted to in-phase and anti-phase operation, then a conventional LLC resonant converter (Fig. 4) can be used as an equivalent circuit where the effective turns ratio is a function of the state of auxiliary switches and the phase-shift between the primary bridges (Table I). Furthermore, the device currents and the winding currents and voltages of the actual circuit can be derived accordingly from the equivalent circuit. Assuming identical tank parameters ($C_{sa} = C_{sb} = C_s$, $L_{sa} = L_{sb} = L_s$ and $L_{ma} = L_{mb} = L_m$), the well-known first harmonic approximation can be used to obtain an expression of the voltage output [12]

$$V_o = \frac{V_{in}}{n_{eff}} \frac{1}{\sqrt{\left(1+\lambda-\frac{\lambda}{f_n^2}\right)^2 + Q^2\left(f_n - \frac{1}{f_n}\right)^2}} \quad (1)$$

TABLE I
VARIATION OF EFFECTIVE TURNS RATIO AND OUTPUT VOLTAGE

Operation	Mode I	Mode II, III	Mode IV
n_{eff}	$n/4$	$n/2$	n
V_o at f_r	$4V_{in}/n$	$2V_{in}/n$	V_{in}/n

where the parameters are defined as follows

$$\text{Resonant frequency, } f_r = \frac{1}{2\pi\sqrt{L_s C_s}} \quad (2)$$

$$\text{Quality factor, } Q = \frac{\pi^2\sqrt{L_s/C_s}}{8\, n_{eff}^2}\frac{P/2}{V_o^2} \quad (3)$$

$$\text{Normalized frequency, } f_n = \frac{f_{sw}}{f_r} \quad (4)$$

$$\text{Inductance ratio, } \lambda = \frac{L_m}{L_s} \quad (5)$$

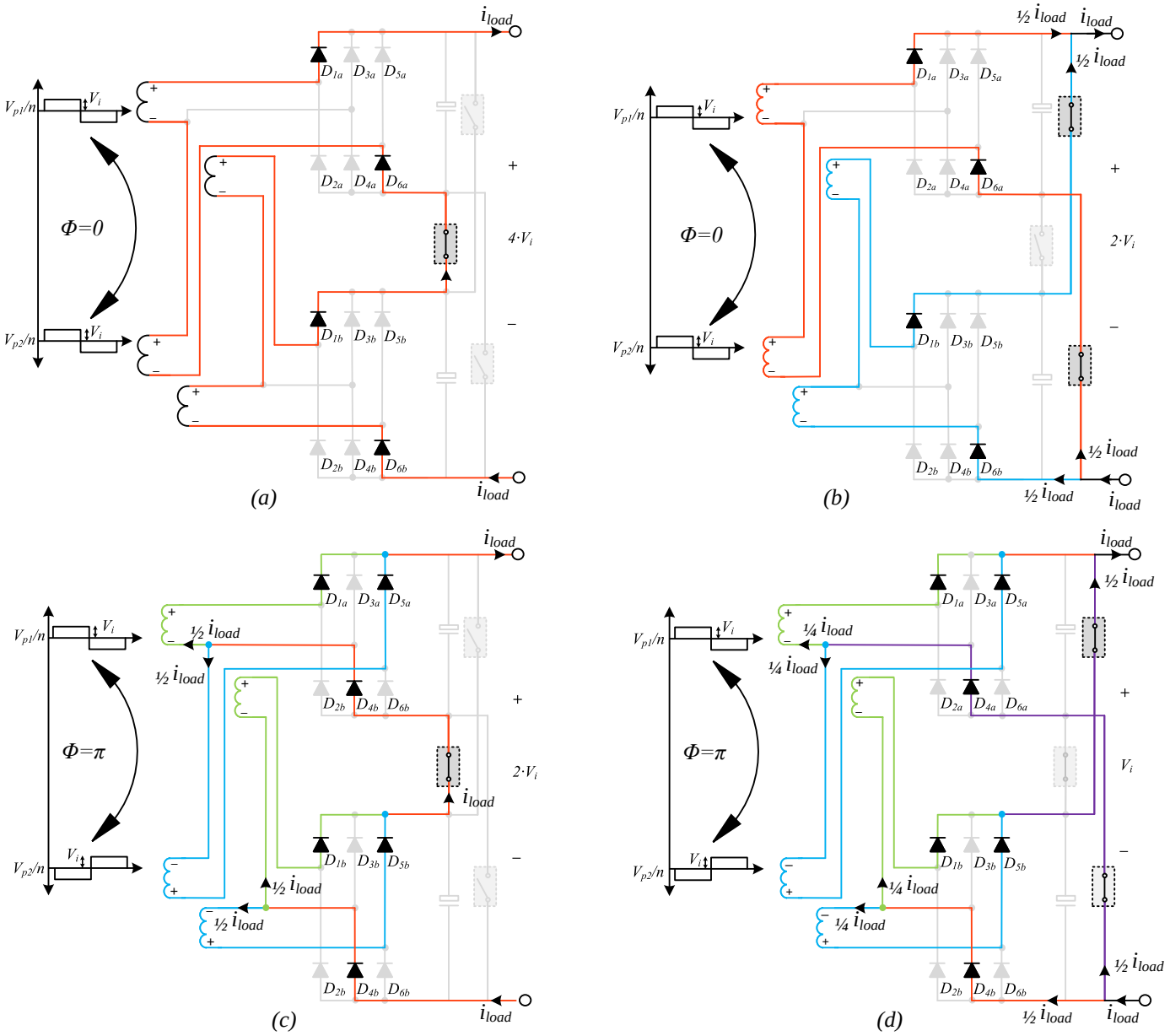

Fig. 3. Secondary-side equivalent circuits (for positive half-cycle of V_{p1}/n) illustrating the effect of phase-shift and auxiliary switch connections on output voltage: (a) Mode I: Series connection with auxiliary switches at zero-phase shift (b) Mode II: Parallel connection with auxiliary switches at zero-phase shift (c) Mode III: Series connection with auxiliary switches under anti-phase operation (d) Mode IV: Parallel connection with auxiliary switches under anti-phase operation

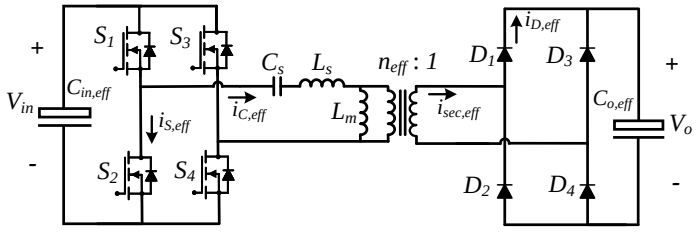

Fig. 4. Equivalent circuit of the converter when the phase-shift between primary side full-bridges is restricted to in-phase and anti-phase operation

III. Results and Analysis

The performance of the converter is illustrated through a simulation study carried out in PLECS. Therein, it is considered that the converter is configured as an LLC resonant circuit (Fig. 2 (a)). The system specifications are listed in Table II.

The steady-state operation of the circuit for the various configurations of Fig. 3 is illustrated in Fig. 5. Therein, the ZVS turn-ON for the MOSFETS can be observed under all operating conditions. The reconfiguration ability of the proposed converter enables the reduction of current stresses on the primary side devices compared to a conventional resonant converter for a given output power and current rating. Additionally, due to

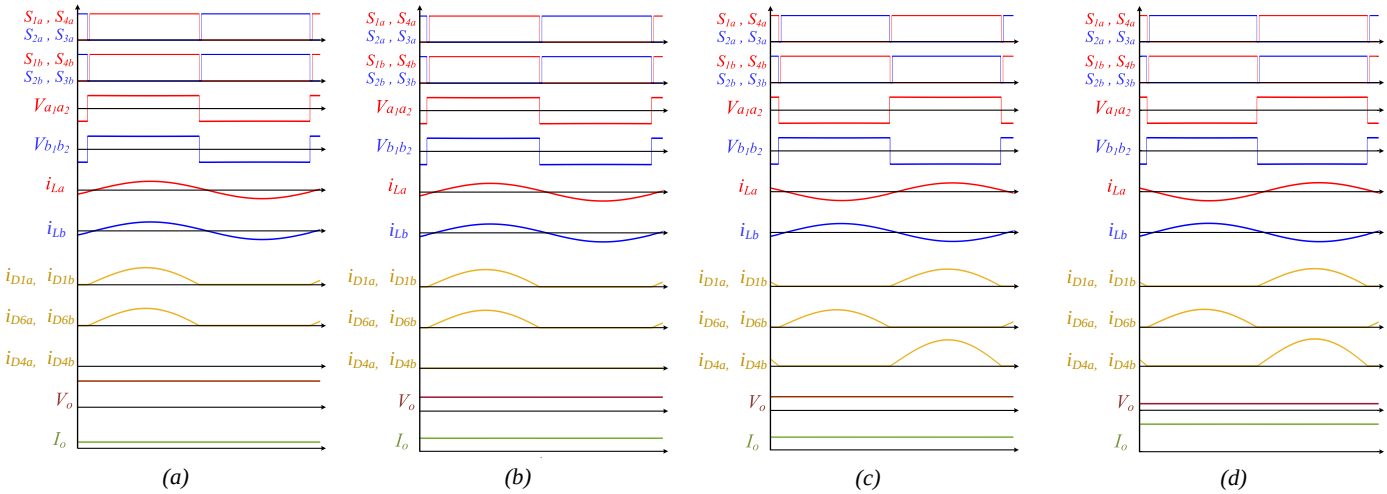

Fig. 5. Waveforms in steady-state for the various operating conditions of Fig. 3: (a) Voltage quadrupling operation (b) Voltage doubling by auxiliary switches (c) Voltage doubling by phase shift (d) Current quadrupling operation; the anti-phase operation governs the conduction of central leg diodes D_{4a} and D_{4b}

TABLE II
SYSTEM PARAMETERS

Parameter	Value
Input voltage, V_{in}	600 V
Switching frequency, f_{sw}	20 kHz
Resonant Capacitance, $C_{s1} = C_{s2}$	650 nF
Effective Series Inductance, $L_{s1} = L_{s2}$	100 μH
Turns ratio, n	1.6:1
Magnetizing Inductance, $L_{m1} = L_{m2}$	1 mH

the presence of auxiliary switches, the voltage stresses on the rectifier diodes and the output capacitances are also halved. Furthermore, the double reconfigurability achieved through phase shift and auxiliary switches ensures the current ratings of the central leg be half and those of the non-central leg be a quarter of the ratings in a conventional resonant converter. These advantages allow the use of semiconductor devices with a much smaller R_{Don} in the converter that can further improve efficiency.

The voltage gain characteristics of the converter for Mode I are shown in Fig. 6 for different values of Q wherein $\lambda = 10$. As is the case with a conventional resonant converter, a lower value of λ can result in narrower gain curves, higher peak voltage, and flexible regulation albeit at the cost of higher magnetizing current, circulation losses, and closed loop stability concerns. In Fig. 7, the gain curves corresponding to different modes are shown. From (1), the dependence of the voltage output on n_{eff} enables an extremely wide range of output (200 V to 1500 V) in a relatively narrow frequency range. Furthermore, it can be inferred from Table I and (2)-(3) that the quality factor of the circuit remains unchanged for constant power output, P, irrespective of the mode of operation. The proposed circuit inherently enables this function since scaling down of output voltage through reconfiguration automatically ensures scaling up of the output current, thereby preventing derating of the converter. Therefore, the points x, y, and z in Fig. 7 represent points of equal output power whereas the corresponding three voltage curves have the same Q of 1. Though the topology appears more complex than a conventional isolated dc-dc converter, these advantages make the design of magnetics simpler since there is a smaller deviation in load-dependent parameters resulting in an optimum choice for the various components.

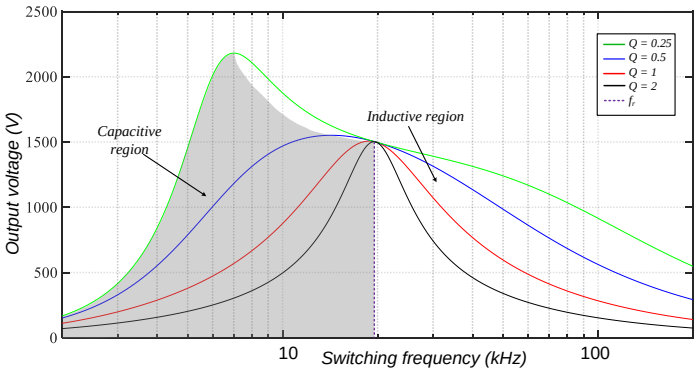

Fig. 6. Variation of output voltage with switching frequency for different values of Q in Mode I

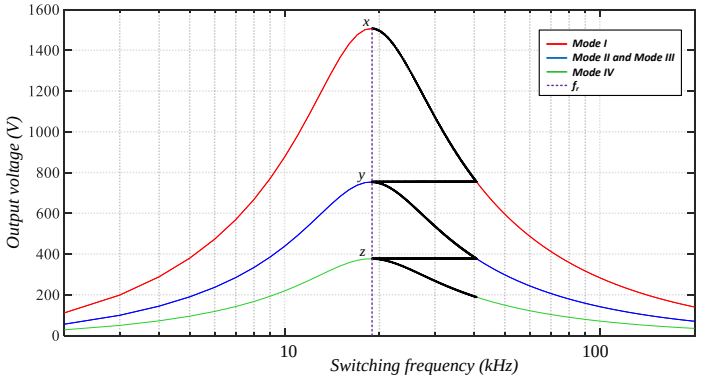

Fig. 7. Variation of output voltage with switching frequency for different modes at Q =1

The main aim of narrowing the frequency range through reconfiguration is to reduce the switching and core losses. This is illustrated in Fig. 8 wherein PLECS thermal models of Wolfspeed C3M0032120D MOSFETs and C4D10120D Schottky diodes are used to form the circuit in Fig. 2 (a) and assess the conduction and switching losses. Alternatively, the semiconductor device and core losses may be approximated analytically [13], [14]. However, for simplicity, the core losses in the simulation are neglected for this analysis. For comparison, a conventional LLC converter is simulated wherein C5D25170H Schottky diodes are used on the rectifier side. Since the resonant converter is controlled through PFM, the two systems are made to operate at identical quality factors to have the same transfer function gain characteristics. Thus, each of the primary side LC tanks and semiconductors theoretically have the same current flow as the conventional converter (Table III).

TABLE III
SPECIFICATIONS FOR THE EFFICIENCY COMPARISON BETWEEN THE CONVENTIONAL LLC CONVERTER AND THE PROPOSED TOPOLOGY

Specification	Conventional	Proposed
Input voltage, V_{in}	600 V	600 V
Output power (max) , P_{out}	22.5 kW	2* 22.5 kW
Avg. input current (max), $I_{in,max}$	37.5 A	2*37.5 A
Turns ratio, n	0.4:1	1.6:1:1

It can be noted that in case the load demand is low, one of the full bridges can be disconnected to avoid underutilization. Therefore, the circuit inherently offers a certain degree of redundancy. Furthermore, the state selection of auxiliary switches and the phase shift between the primary-side bridges can be predetermined prior to initiating power delivery via a communication link in the system. Since power is generally injected into the ship bus fixed at a dc voltage, the reconfiguration-induced transients can never arise. This however does not apply when the converter is used to charge a battery through its complete charging profile such as in EVs. Therefore, in such cases, the design of the converter and choice of reconfiguration mode boundaries becomes more important.

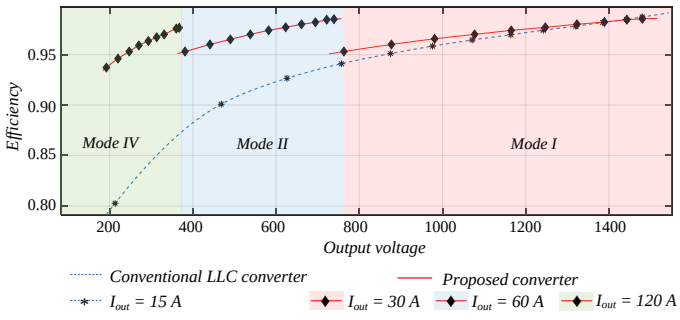

Fig. 8. Efficiency comparison (simulated) of the proposed converter with a conventional LLC resonant converter for wide output voltage; the switching frequency is varied from 20 kHz to 32 kHz for the conventional system and between 20 kHz to 29 kHz for the proposed one

IV. CONCLUSION

In this paper, an isolated DC-DC converter that features an extremely wide output voltage range is proposed. This circuit is capable of dynamic reconfiguration by the use of two primary-side full-bridge converters and two secondary-side three-leg rectifying stages interconnected through auxiliary switches. Collectively, they enable reconfiguration of the rectifying stages equivalently to a voltage/current doubling or quadrupling circuit. The wide operating voltage range makes it suitable for use in SST-based converters for feeding electric ships and boats with different onboard dc voltages. In this work, the operation and steady-state behavior of the converter is explained and via simulation results, it is shown that the proposed converter can operate efficiently over an extremely wide output range. For further work, an analysis of the converter characteristics will be conducted focusing on the derivation of analytical models for the design of the system, and its feedback control strategy. Particular attention will be given to the effects of variation in phase shift, design of magnetics, along with experimental verification.

REFERENCES

[1] K. Kim, K. Park, G. Roh, and K. Chun, "Dc-grid system for ships: a study of benefits and technical considerations," *Journal of International Maritime Safety, Environmental Affairs, and Shipping*, vol. 2, no. 1, pp. 1–12, 2018.

[2] S. Karimi, M. Zadeh, and J. A. Suul, "Shore charging for plug-in battery-powered ships: Power system architecture, infrastructure, and control," *IEEE Electrification Magazine*, vol. 8, no. 3, pp. 47–61, 2020.

[3] S. Qazi, P. Venugopal, G. Rietveld, T. B. Soeiro, U. Shipurkar, A. Grasman, A. J. Watson, and P. Wheeler, "Powering maritime: Challenges and prospects in ship electrification," *IEEE Electrification Magazine*, vol. 11, no. 3, 2023.

[4] H. Tu, H. Feng, S. Srdic, and S. Lukic, "Extreme fast charging of electric vehicles: A technology overview," *IEEE Transactions on Transportation Electrification*, vol. 5, no. 4, pp. 861–878, 2019.

[5] U. Badstübner, "Ultra-high performance telecom dc-dc converter," Ph.D. dissertation, ETH Zurich, 2012.

[6] A. V. Mirtchev and E. C. Tatakis, "Maximum efficiency point tracking algorithm for resonant full-bridge converter in charging applications," *IEEE Transactions on Industrial Electronics*, pp. 1–10, 2023.

[7] A. Elezab, O. Zayed, A. Abuelnaga, and M. Narimani, "High efficiency llc resonant converter with wide output range of 200–1000 v for dc-connected evs ultra-fast charging stations," *IEEE Access*, vol. 11, pp. 33 037–33 048, 2023.

[8] T. B. Soeiro, J. Mühlethaler, J. Linnér, P. Ranstad, and J. W. Kolar, "Automated design of a high-power high-frequency lcc resonant converter for electrostatic precipitators," *IEEE Transactions on Industrial Electronics*, vol. 60, no. 11, pp. 4805–4819, 2013.

[9] D. Zhang and D. Zhang, "Flexible-structured phase-shifted multiple-full-bridge dc–dc power supply with wide range output," *IET Power Electronics*, vol. 9, no. 1, p. 132–141, 2016.

[10] H. Wu, X. Zhan, and Y. Xing, "Interleaved llc resonant converter with hybrid rectifier and variable-frequency plus phase-shift control for wide output voltage range applications," *IEEE Transactions on Power Electronics*, vol. 32, no. 6, pp. 4246–4257, 2017.

[11] F. Grazian, T. B. Soeiro, and P. Bauer, "Voltage/current doubler converter for an efficient wireless charging of electric vehicles with 400 v and 800 v battery voltages," *IEEE Transactions on Industrial Electronics*, pp. 1–11, 2022.

[12] S. De Simone, C. Adragna, C. Spini, and G. Gattavari, "Design-oriented steady-state analysis of llc resonant converters based on fha," in *International Symposium on Power Electronics, Electrical Drives, Automation and Motion, 2006. SPEEDAM 2006.*, 2006, pp. 200–207.

[13] X. Wang, Z. Zhao, K. Li, Y. Zhu, and K. Chen, "Analytical methodology for loss calculation of sic mosfets," *IEEE Journal of Emerging and Selected Topics in Power Electronics*, vol. 7, no. 1, pp. 71–83, 2019.

[14] J. Muhlethaler, J. Biela, J. W. Kolar, and A. Ecklebe, "Improved core-loss calculation for magnetic components employed in power electronic systems," *IEEE Transactions on Power Electronics*, vol. 27, no. 2, pp. 964–973, 2012.